IMPROVED LOCAL COVARIANCE MATRIX REPRESENTATION FOR HYPERSPECTRAL IMAGE CLASSIFICATION

Xinyu Zhang, Yantao Wei, Huang Yao*

School of Educational Information Technology
Central China Normal University
Wuhan, China

Yicong Zhou

Faculty of Science and Technology
University of Macau
Taipa, Macau, China

IGARSS 2020 - 2020 IEEE International Geoscience and Remote Sensing Symposium | 978-1-7281-6374-1/20/$31.00 ©2020 IEEE | DOI: 10.1109/IGARSS39084.2020.9324304

ABSTRACT

This paper proposes a novel spectral-spatial feature representation method for hyperspectral image (HSI) classification. It combines the advantages of adaptive weighted filtering (AWF) and local covariance matrix representation (LCMR) to make full use of the spatial similarity and correlation among different spectral bands. Specifically, the proposed method first uses the maximum noise fraction (MNF) to reduce the dimensionality of HSI. Then, multiscale AWF (MAWF) is applied to make use of spatial information. Next, the spectral-spatial features are obtained by calculating the local covariance matrix of the given pixel and its neighbors. Finally, the learned spectral-spatial features of each pixels are fed into support vector machine (SVM) for classification. Experimental results on two publicly available HSI datasets show that the proposed method is superior to several existing methods in terms of both classification accuracy and classification visual effect, especially when the number of training samples is small.

Index Terms— hyperspectral image classification, adaptive weighted filtering, covariance matrix, feature extraction

1. INTRODUCTION

With the development of hyperspectral imaging technology, more and more information can be captured by hyperspectral cameras. So the abundant information contained in HSI makes it possible to perform more reasonable and effective classification. HSI classification plays an important role in precision agriculture, urban mapping, and environmental monitoring, it has been the focus of many recent research efforts [1, 2, 3].

In HSI classification, the difficulties usually arise from the high dimensionality and insufficient training samples. To solve these problems, many dimension reduction methods have been used in the early stage of research on HSI classification, including principal component analysis (PCA) and maximum noise fraction (MNF). However, these spectral-based dimensionality reduction methods can not obtain satisfied results by using only spectral information.

Therefore, a large number of spectral-spatial feature extraction methods have been designed in the past few years. For example, Kang et al. proposed a spectral-spatial feature extraction method based on edge-preserving filtering (EPF) for HSI classification. In [4], local binary pattern (LBP) has been used to extract local spectral-spatial information. In addition, Zhou et al. proposed a hierarchical framework for extracting spectral-spatial information in HSI [5]. Recently, inspired by the great success of deep learning in the field of computer vision, deep learning methods have also been widely used in HSI classification [1, 6, 7]. The deep learning-based methods usually require a large number of training samples to achieve better performance. However, in the remote sensing field, there is usually only a small amount of labeled data available since the collection of labeled data is either expensive or time-demanding [1].

Recently, Fang et al. [8] proposed local covariance matrix representation for HSI classification. The LCMR-based method achieves better performance in terms of overall accuracy (OA), average accuracy (AA), and Kappa coefficient, especially when the training samples available are limited. However, this method usually produces classification maps with much noise. In order to deal with this problem, improved LCMR (ILCMR) is proposed in this paper. ILCMR can remove salt and pepper noise in the classification maps by combining multiscale AWF (MAWF) with LCMR. The proposed method can extract the spectral-spatial features effectively and enforce a more spatially smooth classification.

The remainder of this paper is organized as follows. In Section II, AWF and CMR are briefly reviewed. Section III describes the proposed ILCMR method for HSI classification. Section IV provides experimental results using two real HSIs. Section V concludes this paper with some remarks at plausible future research.

Yantao wei is the corresponding author. email: yantaowei@mail.ccnu.edu.cn. This work was supported in part by the Natural Science Foundation of Hubei Province under Grant 2018CFB691, the Fundamental Research Funds for the Central Universities under Grant CCNU20TD005, the Science and Technology Development Fund, Macau SAR (File no. 189/2017/A3), and the Research Committee at University of Macau under Grants MYRG2016-00123-FST and MYRG2018-00136-FST.

2. RELATED WORK

2.1. Adaptive weighted filtering

AWF has been widely used in the field of image processing. It can remove noise according to the relationship between the central pixel and the surrounding pixels in the window. Let $\mathbf{X}$ to be original image. $\mathbf{X}_{i,j}$ denotes the gray value of the pixel location (i, j) in image $\mathbf{X}$. Denote $W_{i,j}$ by a $l \times l$ window centered at (i, j). In general, AWF can be defined as

$$\mathbf{X}'_{i,j} = \sum_{m=1}^{l} \sum_{n=1}^{l} W_{i,j}^{m,n} \mathbf{X}_{i,j}^{m,n}, \tag{1}$$

where $\mathbf{X}_{i,j}^{m,n}$ is the gray value of the pixel location (m, n) in the current window, $W_{i,j}^{m,n}$ is the weight in the window centered at (i, j), and $\mathbf{X}'_{i,j}$ is the output of the filter. Note that the weights can be determined by the relationship between the center pixel and its neighbor pixels.

2.2. Covariance Matrix Representation

Assume that we have an image $\mathbf{I}$. For a given region $\mathbf{R} \subseteq \mathbf{I}$ with M pixel. Let $\mathbf{x}_i$ denote the d-dimensional feature extracted from the ith pixel within $\mathbf{R}$, and let μ denote the mean vector of the set of feature vectors $\mathbf{x}_i$ $(i = 1...M)$. The CMR of region $\mathbf{R}$ can be obtained by

$$\mathbf{C}_R = \frac{1}{M-1} \sum_{i=1}^{M} (\mathbf{x}_i - \mu)(\mathbf{x}_i - \mu)^T. \tag{2}$$

Note that the obtained covariance matrix is located on a nonlinear Riemannian manifold space. So the Log-Euclidean-based kernel function can be used to make use of the standard vector space learning algorithm [8].

3. IMPROVED LCMR FOR HSI CLASSIFICATION

Fig.1 shows the flowchart of the proposed method for HSI classification, which consists of the following four steps. First, dimensionality reduction is performed on the original HSI using MNF method, and then MAWF is performed on it. Next, each pixel and its neighboring pixels are extracted in a fixed window to construct LCMR. Finally, the obtained LCMRs are fed into the SVM with Log-Euclidean-based kernel for classification. Our proposed method combines the advantages of MAWF and LCMR.

3.1. Spectral Dimensionality Reduction

In order to remove the noise, dimensionality reduction method is first applied to the original HSI. In this paper, MNF is used as the dimensionality reduction method, since the noise can be effectively removed on the MNF transformed

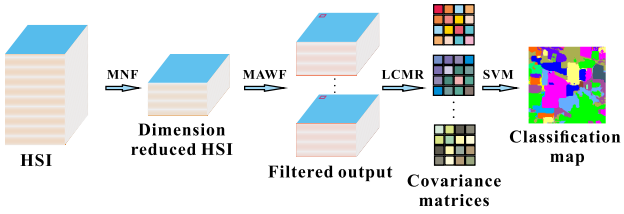

Fig. 1. Flowchart of ILCMR.

space. Let $\mathbf{S}$ and $\mathbf{N}$ are signal component and noise component contained in image data, respectively. The MNF aims to find a linear transformation matrix $\mathbf{A}$ to maximize the SNR of transformed data. $\mathbf{A}$ is the eigenvectors associated with the L largest eigenvalues of $\sum_{\mathbf{N}}^{-1} \sum_{\mathbf{I}}$, where $\sum_{\mathbf{N}}^{-1}$ and $\sum_{\mathbf{I}}$ are the covariance matrix of noise component and original HSI, respectively. Consequently, the dimensionality reduced data $\mathbf{Y}$ can be obtained by $\mathbf{Y} = \mathbf{A}^T \mathbf{I}$ [8].

3.2. Multiscale Adaptive Weighted Filtering

In order to make use of multiscale spatial information, MAWF is adopted in this paper. The central pixel in the filter window can be re-represented according to the weights of its surrounding pixels. We calculate weights with a commonly used Gaussian kernel function. The adaptive weights can be expressed by

$$\mathbf{W}_{i,j}^{m,n} = \frac{\mathbf{F}_{i,j}^{m,n}}{\sum_{m=1}^{l} \sum_{n=1}^{l} \mathbf{F}_{i,j}^{m,n}}, \tag{3}$$

where

$$\mathbf{F}_{i,j}^{m,n} = \exp\left(-\frac{\| \mathbf{Y}_{i,j} - \mathbf{Y}_{i,j}^{m,n} \|^2}{\sigma}\right), \tag{4}$$

where σ is a scale parameter of the Gaussian kernel similarity function. In this paper, MAWF make use of the spectral-spatial characteristics of the HSI. We assume that the input data with size $H \times W \times d$ and let m be the number of filter scales, then the size of the output data is $H \times W \times (d \times m)$.

3.3. Construction of LCMRs

In order to further utilize the information of the spectral image, we can construct LCMR by using a square window of fixed size $P \times P$. For each pixel, $K - 1$ most similar neighboring pixels are extracted by cosine distance measurement. Then we use the total of K pixels including the central pixel to calculate covariance matrix according to (2). Each non-diagonal element in the matrix represents the relationship between different features. In addition, similar pixels in the local space largely represent the same category or the same substance in the HSI, so local covariance matrices obtained by the extracted similar pixels represent the relationships between different spectral features of the same category of substances [8].

3.4. Classification

Finally, the covariance matrices sets are fed into a SVM with Log-Euclidean-based kernel for final classification. The Log-Euclidean-based kernel function is defined by

$$k_{logm}(\mathbf{C}_1, \mathbf{C}_2) = trace[logm(\mathbf{C}_1)\Delta logm(\mathbf{C}_2)], \quad (5)$$

where $\mathbf{C}_1$ and $\mathbf{C}_2$ are two different matrices, $logm$ is the logm operator [8].

4. EXPERIMENTAL RESULTS

In this section, extensive experiments have been conducted to demonstrate the effectiveness of the proposed method. In this paper, five state-of-the-art methods are used for comparison, including superpixel-based classification method via multiple kernels (SC-MK) [9], local binary pattern based method (LBP), edge-preserving filtering-based method (EPF), multiple feature learning based method (MFL) [10], and LCMR. The classification accuracy is illustrated by OA, AA, and Kappa coefficients.

4.1. Data Description

In this paper, two benchmark HSIs are used to verify the effectiveness of the proposed method. The first HSI was gathered by AVIRIS sensor over the Indian Pines test site in North-western Indiana and has the size of $145 \times 145 \times 220$. This data set contains 16 classes. The second HSI is the University of Pavia image. It was collected by the ROSIS sensor over the campus at the University of Pavia, Italy. This scene contains 103 spectral bands after 12 most noisy spectral bands are discarded, and each band has the size of 610×340 pixels. There are 9 kinds of labeled land covers.

4.2. Comparison with Different Methods

The first experiment is performed on the Indian Pines data set and 2% of labeled samples per class are randomly chosen for training, and the remaining are used as test samples. The experimental results including the OA, AA, Kappa and average classification accuracies of each class over 10 repeated experiments are reported in Table 1. It can be observed that the classification accuracy of the proposed method is always better than other comparison methods in terms of OA, AA, and Kappa. The proposed method significantly improves the performance of LCMR. One of the reasons for this is that more spatial information has been exploited by MAWF. The classification results can effectively prove the superiority of the proposed method.

Fig.2 demonstrates classification maps achieved by different methods on the Indian Pines dataset. It can be observed that ILCMR obtains a more homogeneous map than other methods. The proposed method not only has a better smoothing effect, but also retains the boundaries and edges well. The reason for this is that the MAWF and LCMR can not only extract effective spectral-spatial features, but also preserve the structure of HSI. Although the LBP has achieved high classification accuracy, it leads to the over-smoothed classification map.

Table 1. Experimental results on the Indian Pines dataset.

Class	EPF	LBP	MFL	SC-MK	LCMR	ILCMR
1	0.00	74.67	52.00	**100.0**	89.78	80.67
2	76.11	82.97	79.35	90.16	93.72	**95.83**
3	85.19	76.04	75.12	83.89	82.32	**90.48**
4	74.77	70.52	29.91	80.34	75.60	**87.67**
5	89.98	77.29	83.04	78.52	91.08	**91.33**
6	72.74	84.62	93.54	97.66	97.15	**98.85**
7	20.00	95.63	68.52	89.63	**100.0**	**100.0**
8	85.75	92.26	96.94	**100.0**	**100.0**	99.68
9	0.00	70.00	25.79	**100.0**	76.84	**100.0**
10	82.90	79.76	80.47	85.09	83.96	**86.63**
11	70.57	**96.72**	89.69	91.62	93.00	95.60
12	76.08	75.97	66.23	76.75	85.59	**89.57**
13	99.18	77.70	96.90	90.55	99.80	**100.0**
14	86.90	97.52	94.87	96.49	99.86	**99.94**
15	66.68	82.46	74.60	84.66	97.78	**100.0**
16	65.74	61.87	71.54	**98.90**	88.46	91.21
OA	77.14	86.44	83.46	89.69	92.17	**94.76**
AA	65.79	81.02	73.66	90.27	90.93	**94.22**
κ	73.40	84.33	81.06	88.24	91.08	**94.02**

The second experiment is conducted on the University of Pavia dataset, and 1% of labeled samples per class are randomly selected for training. Table 2 reports the experimental results of different methods. The same conclusion can be drawn on this dataset. Fig. 3 shows the classification maps of six methods. It can be visually observed that the edges and boundaries in the map of the ILCMR are in better accordance with the false color composite.

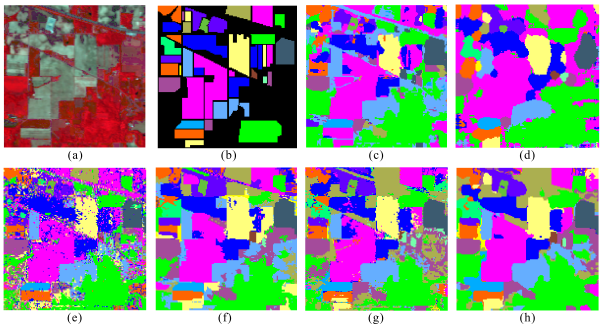

Fig. 2. Classification maps on the Indian Pines dataset. (a) False color composite of the hyperspectral image. (b) ground-truth. (c) EPF. (d) LBP. (e) MFL. (f) SC-MK. (g) LCMR. (h) ILCMR.

Table 2. Experimental results on University of Pavia dataset.

Class	EPF	LBP	MFL	SC-MK	LCMR	ILCMR
1	94.47	87.30	97.18	93.42	95.90	**97.48**
2	94.32	99.36	99.27	95.78	99.44	**99.83**
3	**99.14**	88.25	69.12	91.33	90.60	95.29
4	**99.58**	55.85	86.55	90.01	97.64	97.82
5	99.14	96.00	97.43	99.37	**99.99**	99.74
6	98.08	98.75	92.49	96.99	98.69	**99.31**
7	**98.78**	89.03	94.37	98.23	91.28	93.64
8	85.98	95.90	92.38	75.86	92.09	**98.21**
9	**98.78**	51.32	91.81	99.83	90.90	97.05
OA	94.73	91.97	94.66	93.49	97.18	**98.64**
AA	96.47	94.64	91.18	93.42	95.17	**97.60**
κ	92.92	89.28	92.95	91.42	96.26	**98.20**

5. CONCLUSION

In this paper, ILCMR-based HSI classification method has been proposed. The quantitative results on two publicly available HSI datasets show that the proposed method outperforms several state-of-the-art methods. The proposed method not only takes spectral and spatial information of the HSI into consideration but also overcomes the drawbacks of LCMR. It can obtain high accuracy with limited labeled samples by combining MAWF with LCMR.

In the future, various other HSIs will be used to test the performance of the proposed method. Furthermore, the method of local neighboring pixel construction will be improved.

6. REFERENCES

[1] S. Li, W. Song, L. Fang, Y. Chen, P. Ghamisi, and J.Benediktsson, "Deep learning for hyperspectral image classification: An overview," *IEEE Trans. Geosci. Remote Sens.*, vol. 57, no. 9, pp. 6690–6709, 2019.

[2] J. Aravinth, A. Bharadwaj, K. Harikrishna, and N. Vignajeeth, "Classification of urban objects from hsr-htir data using cnn and random forest classifier," in *Int. Conf. Comm. Elec. Sys. (ICCES)*, Oct 2018, pp. 388–391.

[3] S. Prasad, D. Labate, M. Cui, and Y. Zhang, "Morphologically decoupled structured sparsity for rotation-invariant hyperspectral image analysis," *IEEE Trans. Geosci. Remote Sens.*, vol. 55, no. 8, pp. 4355–4366, Aug 2017.

[4] W. Li, C. Chen, H. Su, and Q. Du, "Local binary patterns and extreme learning machine for hyperspectral imagery classification," *IEEE Trans. Geosci. Remote Sens.*, vol. 53, no. 7, pp. 3681–3693, July 2015.

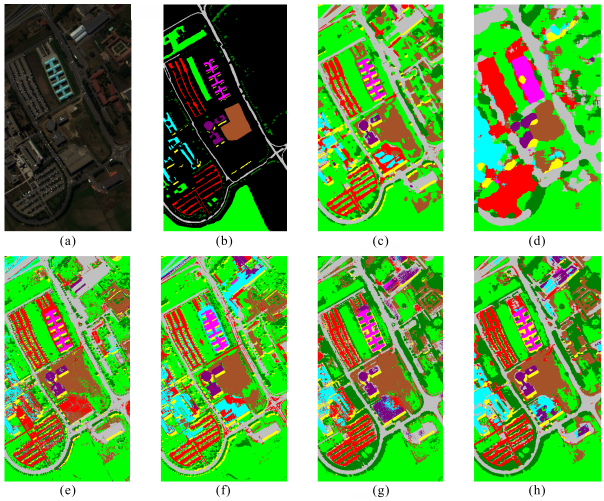

Fig. 3. Classification maps of the University of Pavia dataset. (a) False color composite of the hyperspectral image. (b) ground-truth. (c) EPF. (d) LBP. (e) MFL. (f) SC-MK. (g) LCMR. (h) ILCMR.

[5] Y. Zhou and Y. Wei, "Learning hierarchical spectralcspatial features for hyperspectral image classification," *IEEE Transactions on Cybernetics*, vol. 46, no. 7, pp. 1667–1678, July 2016.

[6] J. Li, Q. Du, B. Xi, and Y. Li, "Hyperspectral image classification via sample expansion for convolutional neural network," in *Works. Hyper. Image. Sig. Process.: Evo. Remote Sens.*, Sep. 2018, pp. 1–5.

[7] X. Han, B. Shi, and Y. Zheng, "Ssf-cnn: Spatial and spectral fusion with cnn for hyperspectral image super-resolution," in *IEEE Int. Conf. Image Process.(ICIP)*, Oct 2018, pp. 2506–2510.

[8] L. Fang, N. He, S. Li, A. J. Plaza, and J. Plaza, "A new spatialcspectral feature extraction method for hyperspectral images using local covariance matrix representation," *IEEE Trans. Geosci. Remote Sens.*, vol. 56, no. 6, pp. 3534–3546, June 2018.

[9] L. Fang, S. Li, W. Duan, J. Ren, and J. A. Benediktsson, "Classification of hyperspectral images by exploiting spectral-spatial information of superpixel via multiple kernels," *IEEE Trans. Geosci. Remote Sens.*, vol. 53, no. 12, pp. 6663–6674, Dec 2015.

[10] J. Li, X. Huang, P. Gamba, J. M. Bioucas-Dias, L. Zhang, J. A. Benediktsson, and A. Plaza, "Multiple feature learning for hyperspectral image classification," *IEEE Trans. Geosci. Remote Sens.*, vol. 53, no. 3, pp. 1592–1606, March 2015.